Vol. 15, No. 3 (2026): 991 - 1006 http://dx.doi.org/10.23960/jtepl.v15i3.991-1006

JURNAL TEKNIK PERTANIAN LAMPUNG

ISSN 2302-559X (print) / 2549-0818 (online)
Journal homepage : https://jurnal.fp.unila.ac.id/index.php/JTP

Rapid Detection of Dragon Fruit Peel Powder Adulteration by Vis-NIR and SW-NIR Spectroscopy with PLSR Model

Nadya Hafidzatun Nisa[1], Rudiati Evi Masithoh[1,✉], Muhammad Fahri Reza Pahlawan[2], Hanim Zuhrotul Amanah[1], Reza Adhitama Putra Hernanda[3]

[1] Department of Agricultural and Biosystems Engineering, Faculty of Agricultural Technology, Universitas Gadjah Mada, Yogyakarta, INDONESIA.

[2] Department of Smart Agriculture Systems, College of Agricultural and Life Science, Chungnam National University, Daejeon, 34134, Republic of Korea.

[3] Department of Biosystems Engineering, College of Agriculture, Life, and Environment Sciences, Chungbuk National University, Cheongju, 28644, Republic of Korea.

Article History:

Received : 14 November 2025
Revised : 09 May 2026
Accepted : 18 May 2026

Keywords:

Adulterant,
DFP powder,
Food authentication,
PLSR,
Spectroscopy.

Corresponding Author:
✉ evi@ugm.ac.id
(Rudiati Evi Masithoh)

ABSTRACT

An important factor in choosing a food product is its quality and safety. Meanwhile, visual aspects are a benchmark for product acceptance. Dragon fruit peel powder (DFP) has excellent potential as a natural food coloring. This study aims to detect adulteration in dragon fruit peel powder using two spectroscopy techniques: Visible-Near Infrared (Vis-NIR) and Shortwave-Near Infrared (SW-NIR) spectroscopy. The adulterants include purple sweet potato flour (PP), erythrosine dye powder (ER), and remazol textile dye powder (TX) with varying concentrations of 0%, 0.5%, 1%, 5%, 10%, 20%, 30%, 40%, 50%, and 100%. Partial least squares regression (PLSR) with ten spectral preprocessing methods was used to analyze data and assess model performance. The results show that combining of spectroscopy with the PLSR model significantly improves accuracy, achieving R^2P values above 0.92 for all adulterants. These findings highlight Vis-NIR and SW-NIR spectroscopy combined with PLSR modeling, as rapid, non-destructive tools. Vis-NIR spectroscopy proved superior to SW-NIR spectroscopy in detecting food colorant adulteration because of its sensitivity to color pigments.

1. INTRODUCTION

Anthocyanin pigments are found in almost all parts of red dragon fruit, both the flesh and the skin. The anthocyanin content in the flesh and skin of dragon fruit is 159.7±8.9 and 135.4±9.3 mg/g of dry sample, respectively, with cyanidin aglycone (which gives it its red-purple color) reaching 12.67±0.63 mg per 100 g of dry sample (Saenjum *et al*., 2021). However, powdered food products are susceptible to adulteration, which can result in economic losses, even threaten consumer health. Adulteration is generally detected using High Performance Liquid Chromatography (HPLC) (Thalhamer & Buchberger, 2019) or UV spectrophotometry, which despite their high sensitivity, require significant investment costs, and the use of hazardous chemical reagents.

As an alternative, non-destructive methods have been developed to authenticate agricultural and food products. Research related to the application of spectroscopy techniques has been conducted, including Vis-NIR spectroscopy in the authentication of paprika powder (Monago-Maraña *et al*., 2021), Fourier Transform Infrared (FT–IR) for detecting coconut sugar adulteration in palm sugar (Roosmayanti *et al*., 2021), and Fourier Transform Near Infrared (FT–NIR)

spectroscopy for detecting adulteration in palm sugar (Rismiwandira *et al*., 2021), which achieved an accuracy level above 80%.

Despite the increasing use of spectroscopic techniques for food authentication, most previous studies have focused on general detection or classification without explicitly considering the role of pigment influenced spectral characteristics. Furthermore, comparative evaluations between different spectral regions, such as Vis–NIR and SW–NIR are still limited and existing approaches rarely establish a comprehensive framework capable of distinguishing between different types of adulteration, including natural substances, food grade, and non-food grade. Therefore, this study proposes a novel approach by integrating pigment driven chemometric analysis with a systematic comparison of Vis–NIR and SW–NIR performance, combined with Partial Least Squares Regression (PLSR) to detect and predict adulteration levels in red dragon fruit peel powder. This research not only advances the application of two types of spectroscopies in natural pigment based food systems but also provides new insights into wavelength dependent sensitivity and a more robust framework for rapid and non-destructive.

2. MATERIALS AND METHODS

2.1. Sample Preparation

The main sample consisted of dragon fruit peel powder adulterated with three types of adulterants: purple sweet potato as a natural ingredient, erythrosine dye (Sunsea brand) as a permitted synthetic ingredient, and textile dye powder (Remazol Red RB) as a prohibited synthetic dye. Dragon fruit peel waste and purple sweet potatoes was purchased from the Colombo market in Sleman, Yogyakarta. Erythrosine dye and textile dye powder were obtained from e-markets in Indonesia.

The preparation of dragon fruit peel (DFP) powder was carried out as described by Eveline & Audina (2019) with modifications. Red DFP was sorted and washed thoroughly, drained, thinly sliced, dried at 60 °C for 15 hours (cabinet dryer Shimizu Scientific Instruments MFG Co., Ltd, Japan). Three adulterants were selected: purple sweet potato (PP) as a natural dye, erythrosine (ER) as a food-grade synthetic dye, and Remazol red RB textile dye (TX) as a prohibited synthetic contaminant. Purple sweet potato flour was prepared by peeling, slicing, soaking, washing, drying at 60 °C for 4 hours (using cabinet dryer). To ensure matrix consistency and minimize physical variance, all powder were ground and sieved through a 100 mesh Tyler CBN Sieve. Adulteration levels were established at 0%, 0.5%, 1%, 5%, 10%, 20%, 30%, 40%, 50%, and 100% (w/w), resulting in 2 g ± 0.05. The mixing process was carried out according to Hernanda *et al*. (2024) using a high-speed vortex for 60 seconds, and each concentration was performed in triplicate. The visual appearance of dragon fruit peel powder that has been adulterated with various types of adulterants, at concentration levels is shown in Figure 1.

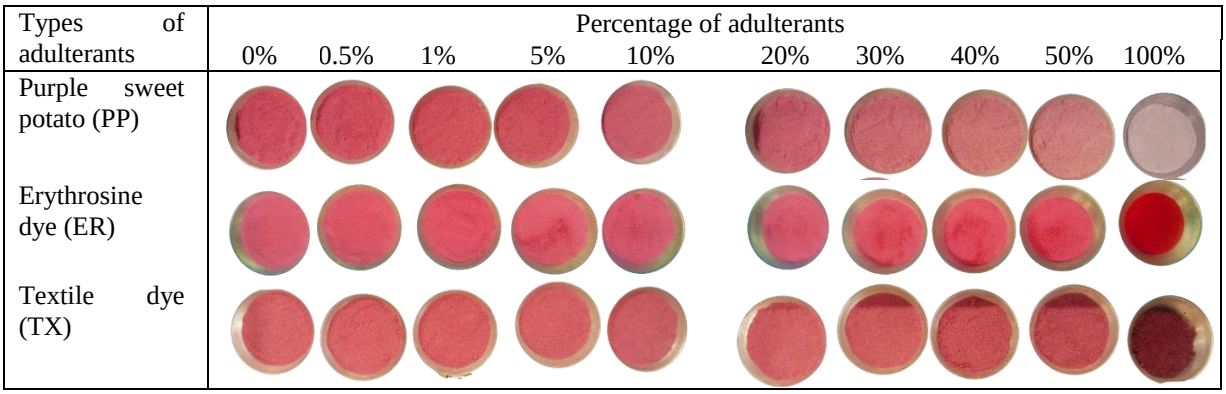

Figure 1. Visual appearance of dragon fruit peel powder that has been adulterated with various types of adulterants at concentration levels

2.2. Measurement of Vis-NIR and SW-NIR Reflectance Spectra

Spectral data were measured in this study using a set of modular spectrometer instruments assembled into a single box, as shown in Figure 2.

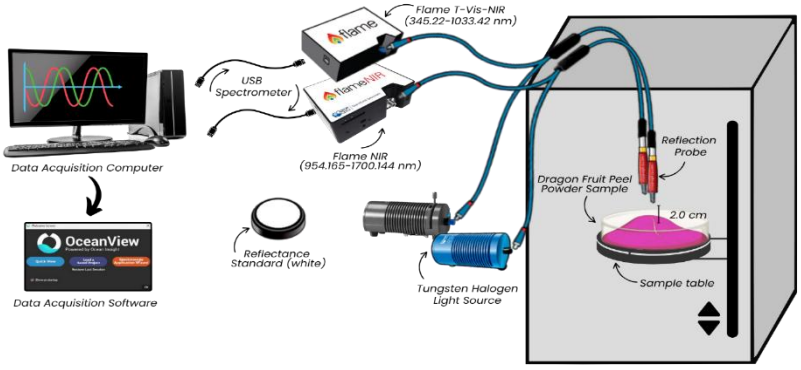

Figure 2. Vis-NIR and SW-NIR spectroscopy instrument

The box consisted of four main instruments, namely a tungsten halogen lamp (HL-2000-HP-FHSA Ocean Optics, 360–2400 nm), a fiber optic reflection probe cable (QR400-7 -VIS-NIR, Ocean Optics), a SW-NIR spectrometer (Flame-NIR-INTSMA25 Ocean Optics, 945.165-1700.144 nm), and a Vis-NIR spectrometer (Flame-T-VIS-NIR Ocean Optics, 345.22-1033.42 nm). The samples were placed 2 cm below the probe on the sample holder. Each sample was scanned at ten different points. For measurements using the miniature Vis-NIR spectrometer, the instrument was set to an integration time of 100 ms, a scan-to-average of 240, and a boxcar width of 2. Meanwhile, for measurements using the miniature SW-NIR spectrometer, the instrument was set to an integration time of 850 ms, a scan-to-average of 20, and a boxcar width of 2.

2.3. Spectral Preprocessing and Multivariate Analysis

The spectral data collected (300 spectra for each adulterant model) were compiled in Microsoft Excel and analyzed in Google Collab for preprocessing and multivariate analysis. The following Python libraries were used: Pandas for data handling, NumPy for numerical operations, Scikit-learn for PLSR and model validation, and SciPy for preprocessing filters. The dataset for each model was divided into a calibration set (70%, n = 210 samples) and a prediction set (30%, n = 90 samples).

Spectral data from Vis-NIR and NIR are inherently complex and often contain a combination of unwanted random noise, physical scatter effects, and baseline variations. Raw spectral data derived from samples such as particle size variance and instrument drift can obscure the underlying chemical information. Therefore, this study evaluates data consisting of seven widely used preprocessing techniques. Four main functional categories of spectral correction were selected to represent preprocessing (Rinnan *et al*., 2009): scatter correction (SNV and MSC), baseline & derivative correction (detrend polynomial, SG1, and SG2), smoothing (smoothing mean), and scaling (mean centering). The empirical comparative approach aims to identify the optimal processing pathway that most effectively isolates chemical information related to impurities from background noise, based on findings in our specific dataset.

Meanwhile, principal component analysis (PCA) was performed as an exploratory data analysis tool to visualize sample clustering and detect potential outliers. PCA was implemented using the Scikit-learn library in a Python environment. To statistically evaluate the sample distribution, 95% confidence ellipses based on the eigenvalues and eigenvectors. This allowed for the identification of potential outliers according to the Hotelling T^2 distribution. Visualization was performed using the Matplotlib library, with the first two principal components (PC1 and PC2) used to represent the maximum variance of the dataset.

Furthermore, the PLSR model was developed on the calibration dataset, using leave-one-out cross-validation (LOOCV) to determine the optimal parameters. The principle of this method is that each sample is alternately

removed from calibration and used for testing. This is a common chemometric approach to spectral data modeling (Lohumi *et al*., 2014). PLSR is highly effective in handling multicollinearity, performs efficiently with small to medium-sized datasets, and is considered a simple and resource-efficient algorithm (Nisa *et al*., 2025). Model performance was assessed using the coefficient of determination for calibration (R^2C), cross-validation (R^2CV), and prediction (R^2P), along with the standard error of calibration (SEC), cross-validation (SECV), and prediction (SEP). Higher R^2 values and lower error values indicate better predictive performance (Masithoh *et al*., 2025). The optimal number of latent variables (LVs) was selected based on the minimum SECV to ensure an appropriate balance between model complexity and predictive accuracy.

In addition, residual prediction deviation (RPD) is used to evaluate model robustness which is calculated as the ratio between the standard deviation of the prediction reference values in the prediction set and SEP. According to commonly accepted criteria in spectroscopic analysis, an RPD value below 2.5 indicates poor prediction, a value between 2.5 and 3.0 indicates prediction accuracy needs to be further improved, and a value above 3.0 reflects excellent prediction performance (Huang *et al*., 2009; Sans *et al*., 2018). The final preprocessing method and model configuration were selected based on their performance on the independent prediction set. The best model was characterized by a high R^2P (close to 1.0), and low SEP (close to 0), RPD > 2.5. Statistical parameters are calculated as follows in Eqs 1- 4 (Zhang D. *et al*., 2019; Zhang M. *et al*., 2019):

$$R^2 = \frac{\sqrt{\sum_{i=1}^{n}(\hat{y}i - yi)^2}}{\sqrt{\sum_{i=1}^{n}(\hat{y}i - ym)^2}} \quad (1)$$

$$SEC = \sqrt{\sum \frac{(\hat{y}i - yi)^2}{n-p}} \quad (2)$$

$$SEP = \sqrt{\sum \frac{(\hat{y}i - yi)^2}{N}} \quad (3)$$

$$RPD = \frac{SD}{SEP} \quad (4)$$

where $\hat{y}i$ and yi represent the measured and predicted adulterant concentrations (%), respectively; ym is the mean reference concentration; SD is the standard deviation of the reference values in the prediction set; and n is the number of samples in the corresponding dataset (calibration, cross validation, or prediction).

3. RESULTS AND DISCUSSION

3.1. Profile of Vis-NIR and SW-NIR Spectra

The original spectra of the DFP powder, erythrosine powder (ER), textile powder (TX), and purple sweet potato flour (PP) samples are shown in Figure 3.

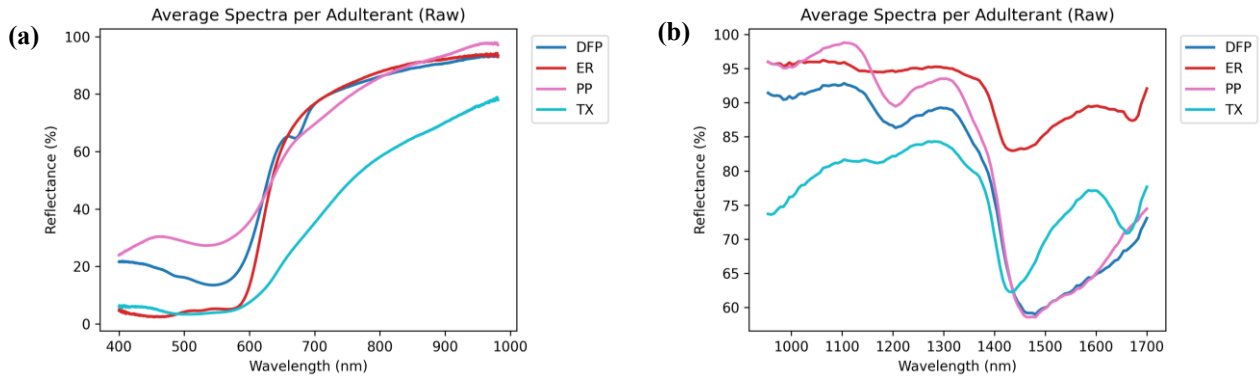

Figure 3. Original spectra using: (a) Vis-NIR spectroscopy, and (b) SW-NIR spectroscopy

Figure 3a shows the spectrum profiles of the samples. The wavelength regions below 450 nm and above 950 nm were excluded from further analysis due to increased noise levels associated with the halogen light source. Halogen lamps exhibit relatively low emission intensity in the short wavelength region and reduce energy output toward the spectral limits, which decreases the signal-to-noise ratio. As a result, spectra in these regions showed unstable baselines and high frequency fluctuations. High reflectance is seen from 600 nm upwards, and high absorbance (low reflectance) can be observed at 450-600 nm due to the presence of anthocyanins (Merzlyak *et al*., 2003) and betalains (Macavilca & Condezo-Hoyos, 2020). Meanwhile, synthetic dyes are designed with strong conjugation systems that yield high absorption in the visible region. Synthetic dyes such as erythrosine B (Acid Red 51; CI 45430) are halogenated xanthene dyes with a xanthene ring as the chromophore center (Pellosi *et al*., 2013). Synthetic dyes such as Remazol red (TX) have maximum absorbance (λmax) in the visible area. This wavelength reflects the electronic transition of the azo chromophore, which produces a characteristic red color (Xiaowei *et al*., 2023). Meanwhile, extending the measurement to SW-NIR can provide additional information about molecular bonds and interactions with the matrix. Figure 3b shows the spectrum profile of the sample using SW-NIR spectroscopy with a wavelength range of 954-1700 nm. SW-NIR spectroscopy performance based on overtones and combined bands from molecular vibrations.

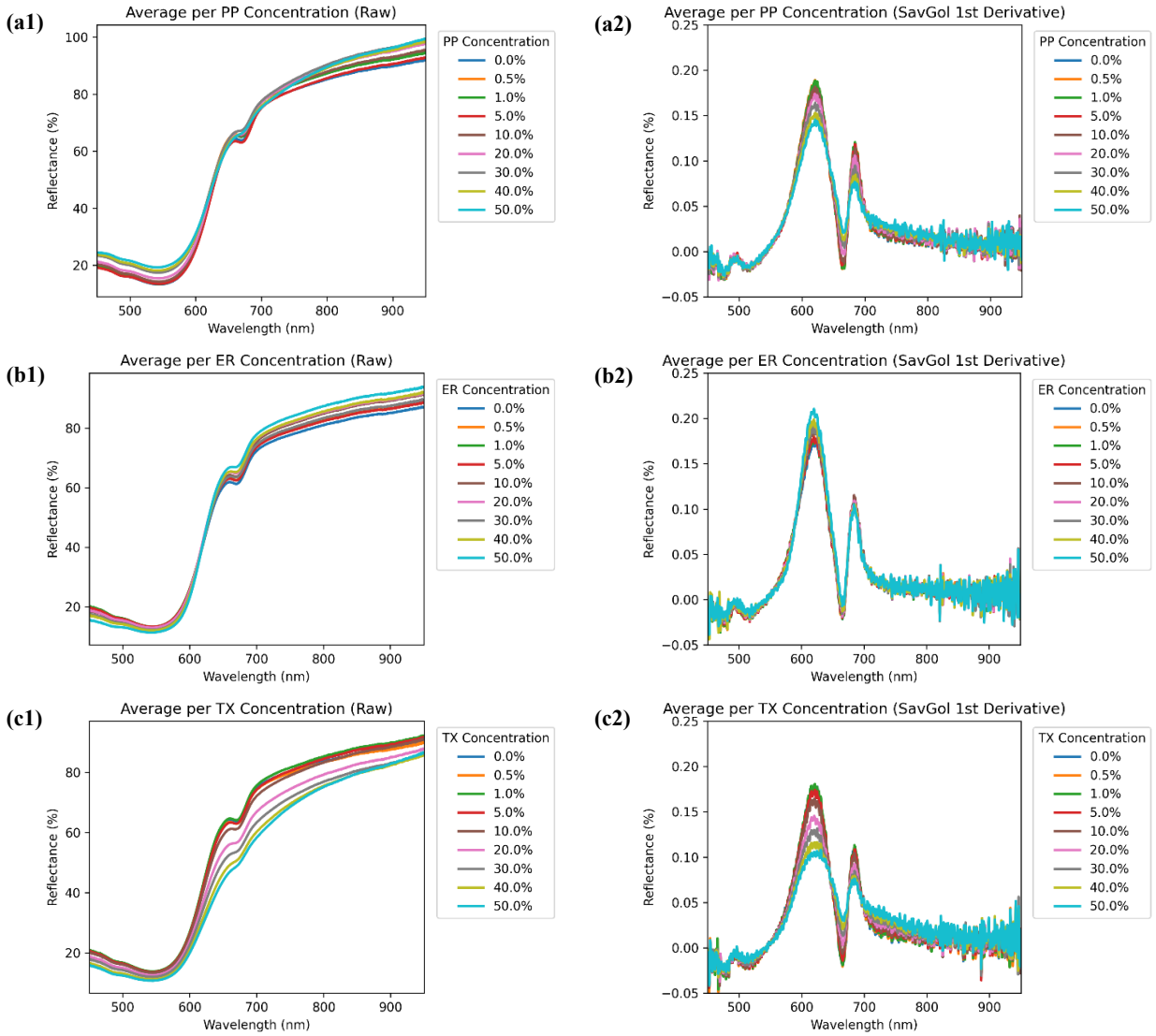

Figure 4. Average Vis-NIR spectra (1) raw and (2) SG1 of dragon fruit peel powder adulterated with: (a) purple sweet potato, (b) erythrosine dye, and (c) textile dye at different concentrations

The average Vis-NIR spectrum shows variations in reflectance that correlate with the active compound content in each sample. Figure 4 illustrates the average Vis-NIR spectra at different adulterant concentrations, which form the basis for the quantitative models. Figure 4 (a1, b1, and c1) shows raw spectra with dominant patterns for color attributes around 450–670 nm, which are related to chromophore transitions in the food matrices. These plots show a clear sequential separation of spectral intensities with increasing adulterant concentration, providing strong visual justification for the use of the quantitative PLSR model. Figure 4 (a2, b2, and c2) shows the same data after Savitzky-Golay 1st Derivative (SG1) preprocessing. This preprocessing effectively removes the broad, sloping baseline and resolves the wide absorption features into sharper, more defined peaks and valleys, thereby isolating specific spectral changes related to concentration.

The average SW-NIR spectrum from adulterated DFP powder is shown in Figure 5. The raw spectra (Fig. 5. a1, b1, c1) again show consistent, ordered changes in reflectance as the adulterant concentration increases, validating the modeling approach. As the SW-NIR spectrum is highly sensitive to organic materials with C–H, O–H, and N–H bonds, the SG1 preprocessing (Fig. 5. a2, b2, c2) highlights these features. Clear absorption peaks are emphasized at 1400–1440 nm (O-H overtone).

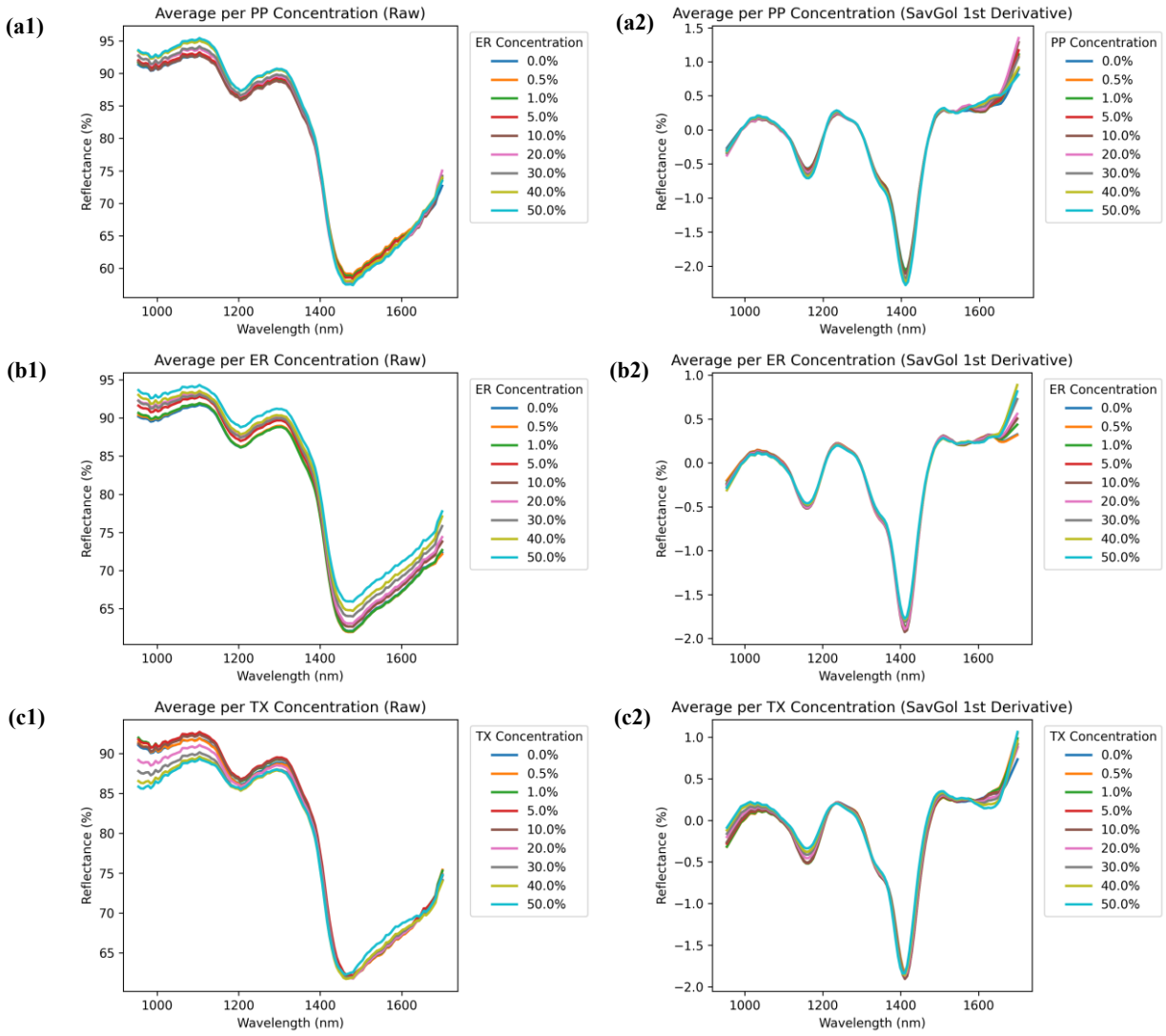

Figure 5. Average SW-NIR spectra (1) raw and (2) SG1 of dragon fruit peel powder adulterated with: (a) purple sweet potato, (b) erythrosine dye, and (c) textile dye at different concentrations

3.2. Results of Principle Component Analysis (PCA)

Global PCA was performed on both the Vis-NIR and SW-NIR datasets to evaluate the natural clustering of samples and ensure data integrity prior to quantitative modeling. Previous studies have used PCA to detect the authenticity of coffee varieties, explaining up to 99.43% of the variance using the first two principal components (PCs) with SW-NIR (Dharmawan & Masithoh, 2025). PCA has also been applied to classify soybeans based on sample type using Vis-NIR, achieving 94% of the variance explained by the first two principal components (PCs) (Abadi *et al*., 2024).

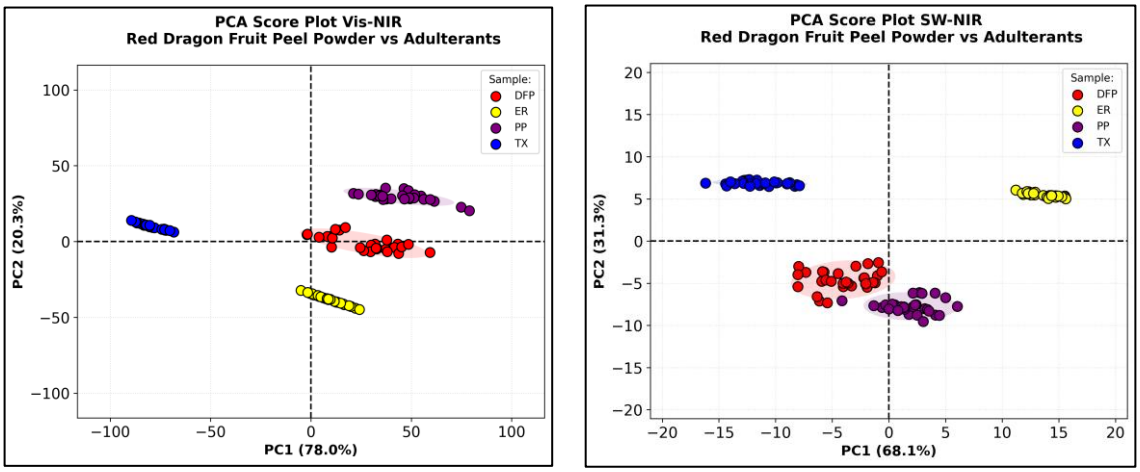

(a) (b)

Figure 6. PCA scores plots of pure and adulterated dragon fruit peel powder samples: (a) Vis-NIR, and (b) SW-NIR regions.

Figure 6 shows the PCA score plots for both spectroscopic methods, where the first two principal components (PC1 and PC2) explain over 98% of the total spectral variance in both cases. In the Vis-NIR region (Figure 6a), PC1 (78.0%) and PC2 (20.3%) provide excellent discrimination between the groups. This separation is primarily due to the different absorption of visible light by synthetic dyes (ER and TX) compared to natural pigments (anthocyanins in the PP and DFP samples). In the SW-NIR region (Figure 6b), a similar level of separation is observed, with PC1 and PC2 explaining 68.1% and 31.3% of the variance, respectively. Clustering in this region highlights differences in molecular vibrations related to C-H, O-H, and N-H bonds between the matrices in the pure samples and various adulterants.

To detect outliers, 95% confidence ellipses (Hotelling's T^2) were applied to the plots. Although most samples clustered tightly, some samples from the PP group on the Vis-NIR plot (Figure 6a) lay slightly outside the 95% confidence limits. However, these points exhibit low Q residuals, indicating that they are well-explained by the model and likely represent natural variation within the sample matrix. Therefore, all samples were retained to ensure the robustness and realistic variability of the subsequent PLSR model.

3.3. Result of PLSR from Vis-NIR Spectra

A partial least squares regression (PLSR) model was developed to quantify the concentration of each adulterant using the Vis-NIR spectra. The statistical metrics generated from this evaluation are presented in Table 1.

A comparative analysis in Table 1 shows that pre-processing significantly impacts model performance. Standard Normal Variation (SNV) was identified as the optimal method for three adulterants, which can be understood through the spectral characteristics of the powder matrix. In this study, DFP powder was sieved to 100 mesh, but residual inter-replica variability in particle arrangement and surface roughness within the sample container remained. This is a known source of multiplicative scattering variance in miniaturized spectrometer configurations (Vera *et al*., 2025). SNV corrects this multiplicative distortion by standardizing each individual spectrum independently by subtracting its mean value and dividing by its standard deviation thus normalizing the spectral intensity without changing the relative shape of the chemical absorption features (Rinnan *et al*., 2009). The reduction in latent variables (LVs) when SNV is

applied to TX detection (from 8 to 4) supports this interpretation, as fewer LVs are needed to represent the underlying chemical variance after physical scattering artifacts are removed (Lanjewar *et al*., 2024; Lukacs *et al*., 2024a).

Table 1. Performance of the PLSR Vis–NIR model using raw spectrum data and various pre-processing methods

Sample	Preprocessing	R^2C	SEC	R^2CV	SECV	R^2P	SEP	RPD	LVs
Purple Sweet Potato (PP)	Raw	0.99	1.36	0.99	1.76	0.99	1.58	11.14	8
	MSC	1.00	1.14	0.99	1.51	0.99	1.47	11.98	7
	SNV	1.00	1.13	0.99	1.51	0.99	1.45	12.21	7
	SavGol 1st Derivative	0.99	1.45	0.98	2.40	0.99	2.15	8.20	7
	SavGol 2nd Derivative	0.98	2.37	0.52	12.28	0.57	11.68	1.51	10
	Smoothing Mean	0.99	1.45	0.99	1.75	0.99	1.53	11.56	8
	Detrend Polynomial (deg=2)	0.99	1.29	0.99	1.73	0.99	1.69	10.42	7
	Mean Centering	0.99	1.36	0.99	1.76	0.99	1.58	11.14	8
Erythrosine dye (ER)	Raw	0.99	1.58	0.96	3.73	0.96	3.32	5.32	11
	MSC	0.99	1.94	0.96	3.66	0.97	3.21	5.50	8
	SNV	0.99	1.85	0.96	3.50	0.97	3.16	5.59	8
	SavGol 1st Derivative	0.96	3.64	0.89	5.91	0.87	6.50	2.72	5
	SavGol 2nd Derivative	0.77	8.51	0.49	12.65	0.45	13.13	1.34	4
	Smoothing Mean	0.99	2.01	0.95	3.79	0.97	3.18	5.55	11
	Detrend Polynomial (deg=2)	1.00	1.01	0.96	3.71	0.96	3.55	4.97	11
	Mean Centering	0.99	1.58	0.96	3.73	0.97	3.32	5.32	11
Textile dye (TX)	Raw	1.00	0.88	0.99	1.36	1.00	1.19	14.79	8
	MSC	1.00	1.12	0.99	1.45	0.99	1.26	13.98	5
	SNV	1.00	1.18	0.99	1.37	1.00	1.12	15.82	4
	SavGol 1st Derivative	1.00	0.18	0.99	1.95	0.99	1.80	9.79	15
	SavGol 2nd Derivative	0.30	14.78	-0.03	17.97	0.03	17.46	1.01	1
	Smoothing Mean	1.00	1.08	0.99	1.36	1.00	1.21	14.55	7
	Detrend Polynomial (deg=2)	1.00	1.00	0.99	1.43	0.99	1.42	12.42	6
	Mean Centering	1.00	0.88	0.99	1.36	1.00	1.19	14.79	8

Furthermore, Figure 7 shows the regression coefficients (β-coefficients) of the optimal PLSR model for each adulterant. Regression coefficients can interpret the relationship between a particular band and the chemical content of the sample (Masithoh *et al*., 2024) and identify which wavelengths contribute most to the prediction data (y-variable).

Absorbance peaks corresponding to anthocyanins or betacyanins were observed at wavelengths of 500–600 nm (Ambrose & Cho, 2014) and 635 nm (Guo *et al*., 2016). This is consistent with Figure 7a (PP model), which shows a peak at 620–640 nm, indicating a high anthocyanin content. The presence of these peaks is likely due to the dominant anthocyanin or betacyanin content in dragon fruit skin. At wavelengths between 700–710 nm, there is an absorbance peak correlated with anthocyanin or O-H stretching (Amanah *et al*., 2020; Saputri *et al*., 2022). A reflectance peak also correlated with O-H stretching can be seen at a wavelength of 930 nm (Fernández-Novales *et al*., 2009). In Figure 7b, shows a xanthene erythrosine ring system that has a peak at 532 nm and strongly absorbs green light, making it appear red and clearly detectable in the spectral range of Vis (Batistela *et al*., 2011). Meanwhile, the synthetic Remazol red (TX) dye, as shown in Figure 7c, has an absorbance peak at 519 nm, reflecting the electronic transition of the azo chromophore that produces a characteristic red colour (Xiaowei *et al*., 2023).

The sensitivity of the Vis-NIR model was quantified through LOD values of 4.73% (PP), 12.11% (ER), and 4.47% (TX), with corresponding LOQ values as shown in Figure 8. A specific study on infant formula has shown that NIR spectroscopy can achieve LODs below 1 ppm for certain chemicals such as melamine (Wang *et al*., 2018). In this study, the detection limits of 4–12% observed for DFP powder remained highly effective for rapid laboratory-scale screening. This difference is primarily due to the higher spectral complexity of the natural fruit peel matrix compared to standard milk ingredients.

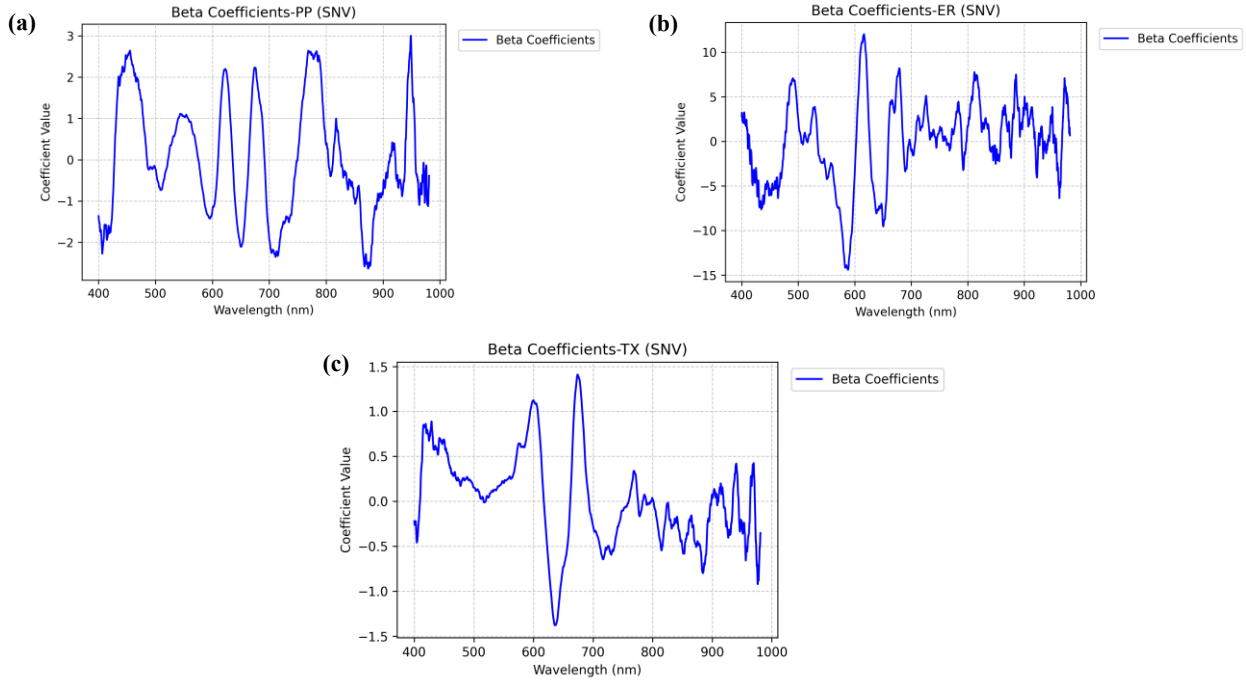

Figure 7. β-coefficients from PLSR models based on Vis–NIR spectra for adulterant detection: (a) purple sweet potato, (b) erythrosine dye, and (c) textile dye

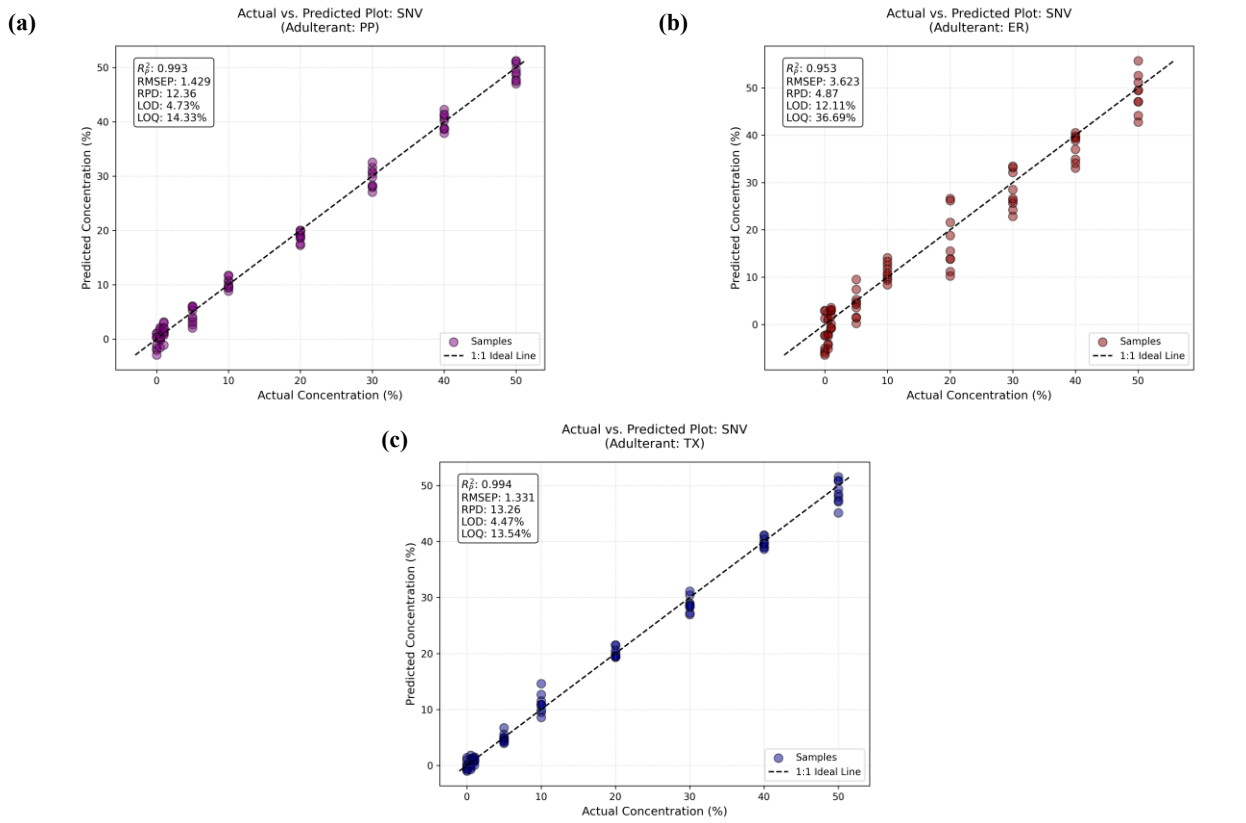

Figure 8. Correlation plots between actual and predicted concentrations (%) of: (a) purple sweet potato, (b) erythrosine dye, and (c) textile dye using Vis-NIR spectroscopy

3.4. Results of PLSR from SW-NIR Spectra

The shortwave near-infrared spectrum is highly sensitive to the concentration of organic materials that have C-H, O-H, and N-H bonds. The results of the PLSR analysis based on SW-NIR spectral data with raw data and optimal preprocessing are shown in Table 2.

Table 2. Performance of the PLSR SW-NIR model using raw spectrum data and various pre-processing methods

Sample	Preprocessing	R2C	SEC	R2CV	SECV	R2P	SEP	RPD	LVs
Purple Sweet Potato (PP)	Raw	0.99	1.79	0.95	4.59	0.98	2.33	7.57	15
	MSC	0.99	2.02	0.93	5.12	0.98	2.56	6.90	15
	SNV	0.99	2.00	0.93	5.24	0.98	2.53	6.99	15
	SavGol 1st Derivative	0.98	2.22	0.95	4.76	0.98	2.59	6.82	8
	SavGol 2nd Derivative	0.96	3.41	0.95	4.24	0.96	3.63	4.86	5
	Smoothing Mean	0.99	2.15	0.95	4.61	0.98	2.57	6.88	17
	Detrend Polynomial (deg=2)	0.99	1.96	0.96	4.13	0.97	2.81	6.28	16
	Mean Centering	0.99	1.79	0.95	4.59	0.98	2.33	7.57	15
Erythrosine dye (ER)	Raw	0.92	5.05	0.90	5.58	0.94	4.38	4.03	7
	MSC	0.94	4.28	0.90	5.67	0.92	5.11	3.45	9
	SNV	0.94	4.16	0.90	5.53	0.92	4.99	3.54	9
	SavGol 1st Derivative	0.94	4.30	0.90	5.61	0.93	4.59	3.84	17
	SavGol 2nd Derivative	0.93	4.52	0.89	6.03	0.93	4.54	3.89	14
	Smoothing Mean	0.93	4.63	0.90	5.65	0.94	4.45	3.97	15
	Detrend Polynomial (deg=2)	0.94	4.32	0.89	5.86	0.93	4.54	3.89	9
	Mean Centering	0.92	5.05	0.90	5.58	0.94	4.38	4.03	7
Textile dye (TX)	Raw	0.99	1.29	0.99	1.45	0.99	1.50	11.80	8
	MSC	0.99	1.58	0.99	1.75	0.99	1.79	9.85	6
	SNV	1.00	1.24	0.99	1.45	0.99	1.54	11.47	7
	SavGol 1st Derivative	0.99	1.40	0.99	1.56	0.99	1.64	10.74	6
	SavGol 2nd Derivative	0.99	1.27	0.99	1.70	0.99	1.75	10.06	15
	Smoothing Mean	0.99	1.28	0.99	1.46	0.99	1.63	10.84	10
	Detrend Polynomial (deg=2)	1.00	1.14	0.99	1.78	0.99	1.92	9.18	14
	Mean Centering	0.99	1.29	0.99	1.45	0.99	1.50	11.80	8

As shown in Table 2, Mean Centering was selected as the most optimal pre-processing method for the SW–NIR dataset. The relatively high LV count in the optimal SW–NIR PP model (LV = 15 with Mean Centering) requires explicit justification and overfitting assessment. The elevated LV count reflects the fundamental spectral characteristics of the SW–NIR region. The R^2C and R^2CV gap for the PP optimal model is 0.04 (0.99 vs. 0.95), and R^2P (0.98) closely matches R^2CV confirming that LOOCV correctly estimates the model's true predictive power and that performance does not collapse on unseen data, which is the defining of overfitting (Rinnan *et al*., 2009). The stability accuracy trade-off is most clearly demonstrated by comparing non-optimal high-LV configurations against the optimal model: the Smoothing Mean preprocessing (LV = 17) and MSC/SNV (LV = 15) for PP yield RPD = 6.88–6.99 compared to RPD = 7.57 for Mean Centering (LV = 15), showing that the SECV minimum criterion selects LV counts that maximize predictive utility rather than calibration fit. Conversely, reducing LVs below the minimum SECV threshold through SG2 preprocessing (LV = 5), yields a less accurate and less stable model. These results collectively demonstrate that the observed LV range (7–15) reflects the spectral dimensionality of a broadband vibrational dataset for a multi-component food matrix, and not model overfitting (Nisa *et al*., 2025; Vera *et al*., 2025). These vibrational-based bands are intrinsically weaker and more spectrally diffuse compared to their fundamental transitions, as they represent forbidden anharmonic overtones with significantly lower molar absorptivity (Beć *et al*., 2018; Singh *et al.,* 2021). Consequently, the inherently low intensity of these overlapping signals makes them highly susceptible to scatter effects, thus requiring robust spectral pre-processing to extract meaningful analytical information (Rinnan *et*

al., 2009). Therefore, the dominant systematic artifact in the SW–NIR measurements in this study is not multiplicative scattering, which is substantially reduced by the uniform 100-mesh filtering protocol, but rather a flat or slowly varying additive offset or spectral shift of the entire spectrum caused by small instrument thermal drifts, variations in ambient illumination, or small differences in fiber optic probe repositioning between measurement sessions (Rinnan *et al*., 2009; Vera *et al*., 2025). Mean Centering eliminates this systematic additive effect by subtracting the column-averaged spectrum from all spectra in the dataset, thereby centering the data at zero variance without amplifying high-frequency noise or distorting the weak but chemically consistent absorption patterns that characterize the DFP matrix and its adulterants (Masithoh *et al*., 2025; Rinnan *et al*., 2009). The absence of additional improvement from multiplicative scattering correction methods such as SNV or MSC that showed RPD values lower or equal to the Raw model for SW–NIR (Table 2) further confirms that scattering heterogeneity is not a major source of variance in the SW–NIR dataset under the controlled measurement conditions in this study, consistent with the observation by Lukacs *et al*. (2024b) for protein powder matrices measured with a miniature SW–NIR spectrometer. The beta coefficients (β-coefficients) of the SW-NIR model (using Mean Centering) are shown in Figure 9, which identifies the wavelengths with the most significant influence on the PLSR model. Strong relationships are indicated by high coefficient values (peaks and valleys) (Saputri *et al*., 2022).

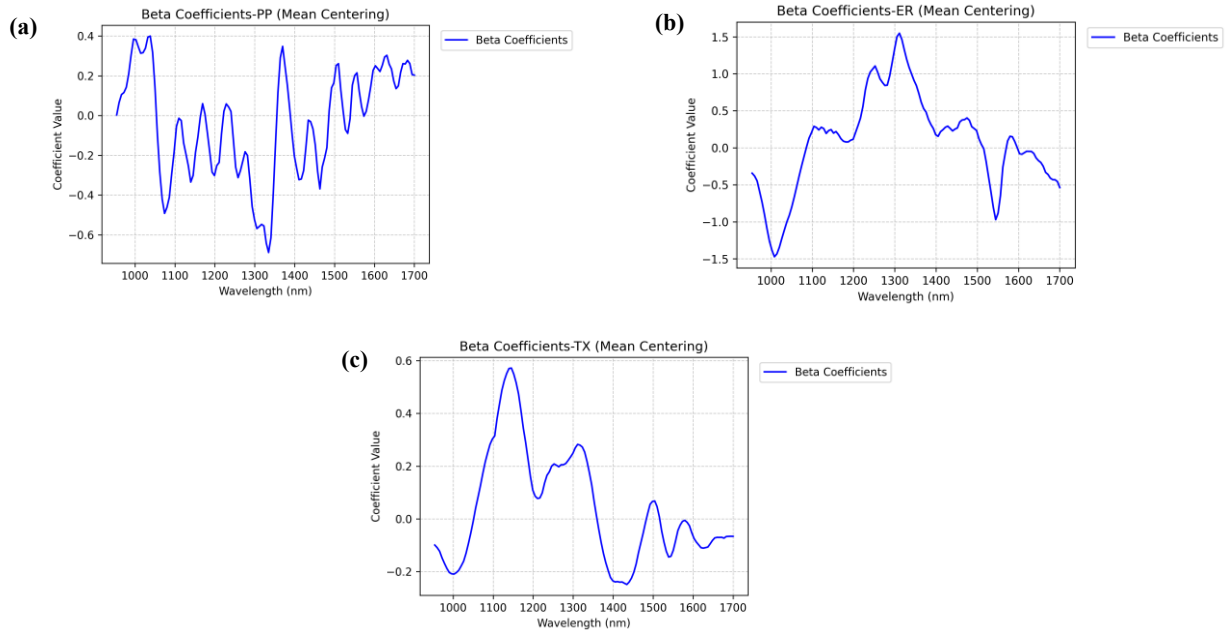

Figure 9. β-coefficients from PLSR models based on SW–NIR spectra for adulterant detection: (a) purple sweet potato, (b) erythrosine dye, and (c) textile dye

Several peaks were recorded between 1428–1470 nm, which are closely related to the first overtone of O-H stretching, indicating water content (Lúcia *et al*., 2017). Additional absorption bands between 1362–1388 nm are related to C-H combination vibrations, while peaks around 1300–1500 nm can be associated with the second overtone of sugars (such as sucrose, glucose, and fructose) (Huang *et al*., 2009). Another significant peak at 1250 nm is caused by the second overtone of C-H stretching, which has been associated with the structure of anthocyanin compounds (ElMasry *et al*., 2011).

This indicates that in the SW-NIR wavelength region, the model detects changes in chemical composition related to water content, sugar content, and organic pigments. In the SW-NIR region, the predictive performance and sensitivity are depicted in Figure 10, which shows LODs of 4.80% for TX and 8.99% for PP, while the ER model is significantly less sensitive with an LOD of 16.92%. The higher LODs for synthetic dyes compared to the Vis-NIR range are due to the lack of unique vibrational signatures in the shortwave region isolated from the DFP matrix.

Compared with other NIR spectrometers, which can achieve LODs of around 0.1%-1.0% for nitrogen-based adulterants in protein powders (Lukacs *et al*., 2024b), milk powder (Henn *et al*., 2017), and whey protein (Lukacs *et al*., 2018), the higher limits observed in this study are attributed to the higher complexity of the fruit peel matrix and the spectral diffuse nature of the overtones in the miniaturized detector configuration. Despite these limitations, the SW-NIR model remains very robust for detecting starch-based adulterants such as PP flour, which provides a strong correlative basis for the model by substantially altering the bulk molecular functional group composition of the DFP mixture.

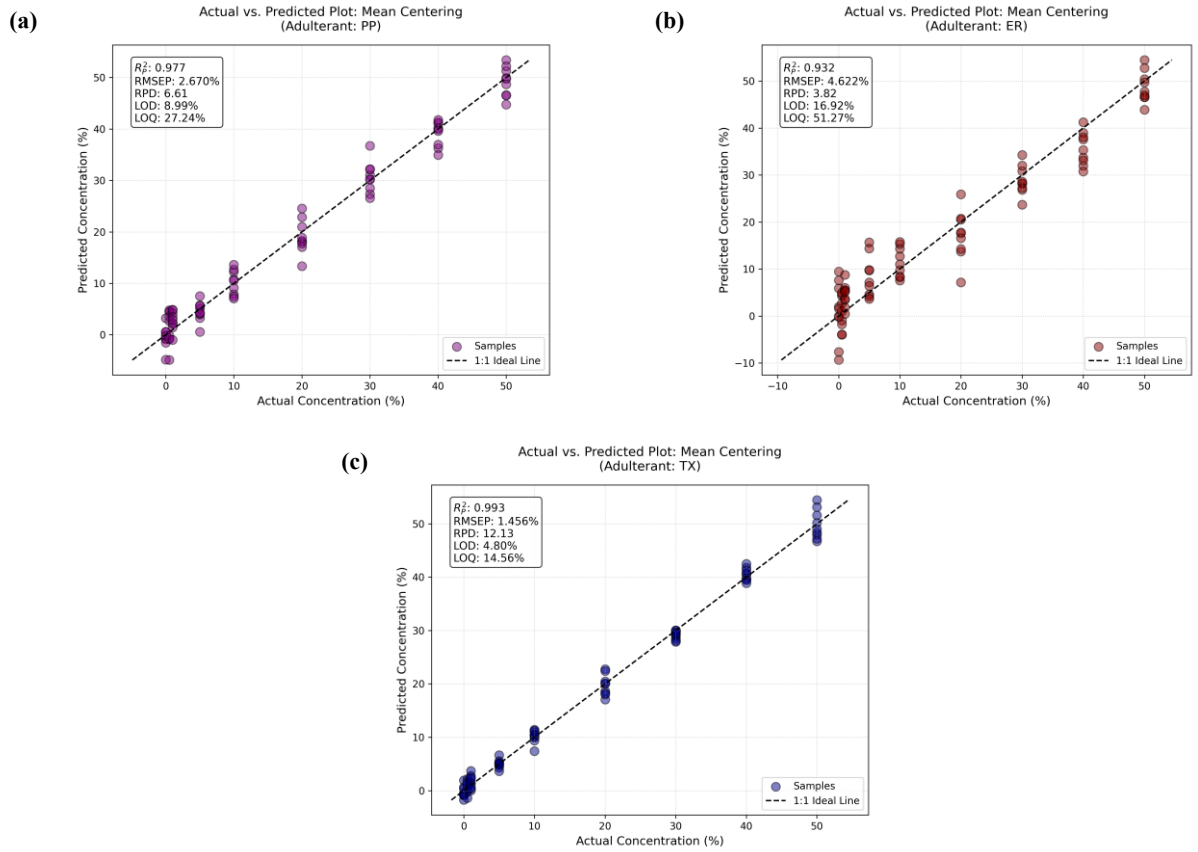

Figure 10. Correlation plots between actual and predicted concentrations (%) of: (a) purple sweet potato, (b) erythrosine dye, and (c) textile dye using SW-NIR spectroscopy.

3.5. Performance Comparison of Vis-NIR and SW-NIR Spectroscopy

The fundamental differences in detection mechanisms between Vis–NIR and SW–NIR for specific authentication tasks are not interchangeable in detecting these adulterants. Both spectral ranges operate through different analytical principles. The Vis–NIR model (450–950 nm) functions as a chemically selective system, where each of the three adulterants has a strong and distinct electronic absorption transition in the visible range that can be spectrally separated from the background of the DFP matrix. Anthocyanins and betacyanin in PP exhibit characteristic absorption peaks at 530–640 nm (Macavilca & Condezo-Hoyos, 2020; Merzlyak *et al*., 2003), erythrosine (ER) absorbs maximally at 532 nm via its halogenated xanthene chromophore (Batistela *et al*., 2011), and Remazol red (TX) exhibits an absorption maximum at 519 nm from the electronic transition of its azo chromophore (Xiaowei *et al*., 2023). These peaks can be directly and uniquely attributed to the molecular identity of the impurities, rather than to the matrix. The β coefficient plot (Figure 7) confirms the finding that prominent charges appear precisely at the specific wavelength of the chromophore of each impurity, indicating that the PLSR model utilizes a direct spectral fingerprint of the electronic structure of each compound. This is consistent with the well-established behavior of Vis–

NIR spectroscopy for the authentication of natural pigment-based foods, as reported for anthocyanin-rich matrices such as red beet powder (Masithoh *et al*., 2024, 2025) and quinoa (Macavilca & Condezo-Hoyos, 2020).

In contrast, the SW–NIR (954–1700 nm) model is best characterized as a compositional correlation system. In this spectral range, none of the three adulterants has an absorption band that is spectrally isolated from the background of the DFP matrix and can be separated at the spectral resolution of the SW–NIR spectrometer used. The SW–NIR region encodes overtone bands and O–H, C–H, and N–H bond combinations that are common to all organic food matrices (Rinnan *et al*., 2009; Vera *et al*., 2025). When a PP forger is added to DFP powder, there will be additional C-H bonds derived from starch and polysaccharide O-H groups (1300–1500 nm, 1400–1440 nm) (Chen *et al*., 2024) while displacing aromatic C–H overtones associated with anthocyanins (1143–1163 nm; 1250 nm) (Amanah *et al*., 2020; ElMasry *et al*., 2011). Thus, the SW–NIR PLSR model detects adulterant concentration as an indirect proxy for this overall compositional transformation, rather than as a direct spectral signature of the unique molecular structure of the adulterant. This is in accordance with the compositional correlation NIR models described for cereal flour substitution, where the models capture changes in the starch-to-protein or moisture-to-fiber ratio, rather than the spectra of specific adulterants (Lohumi *et al*., 2014; Vera *et al*., 2025). Therefore, in terms of the specific authenticity of DFP powder against color-based contaminants, Vis-NIR spectroscopy is a superior method.

3.6. Limitations and Practical Implications

While promising performance was achieved in this study, several limitations exist. First, the dataset was developed under highly controlled laboratory conditions, including a single batch of raw materials, relatively uniform particle size, a single instrument, and a single measurement session. While this design is suitable for proof-of-concept, it may limit the robustness of the developed model when applied to more variable real-world conditions. Variations in raw material origin, processing method, particle size distribution, and instrument configuration are known to significantly affect the spectral response and stability of the model, potentially leading to decreased prediction accuracy. Furthermore, the model has not been validated across multiple batches, time periods, or instruments. For practical applications, robust spectroscopic models require external validation to ensure transferability and reproducibility. Approaches such as multi-batch calibration, instrument standardization, and model update strategies are needed to improve model generalization and reliability. Further development is needed before real-time implementation can be achieved. This includes expanding the dataset to encompass a wider range of variability and evaluating model performance under industrial processing conditions. Therefore, future studies are expected to focus on large-scale validation and system optimization to bridge the gap between laboratory feasibility and industrial applications.

4. CONCLUSIONS

This study successfully demonstrated the capability of Vis-NIR and SW-NIR spectroscopy combined with PLSR modeling for rapid and non-destructive quantification of dragon fruit peel (DFP) powder adulterated with purple sweet potato (PP), erythrosine (ER), and textile dye (TX). Initial exploration analysis using PCA effectively discriminated all sample groups, with 95% confidence ellipses confirming a robust dataset free of significant outliers. The main findings concluded that the Vis-NIR spectral was definitively superior to the SW-NIR for the task of authenticating this natural pigment. The optimal Vis-NIR model was developed using SNV preprocessing, achieving excellent prediction accuracy. These models achieved high R^2P values ($R^2P = 0.97$ for ER, and $R^2P \geq 0.99$ for PP and TX) and robust RPD values (12.21 for PP, 5.59 for ER, and 15.82 for TX). While the SW-NIR model (using Mean Centering) remained effective, they exhibited lower robustness, especially for synthetic dyes (e.g., RPD = 4.03 for ER). Vis-NIR spectroscopy excels directly measuring the main chemical “fingerprint” of impurities, namely color-based chromophores, which are clearly identified in the beta coefficient plots at 519 nm and 532 nm. The SW-NIR models were limited to detecting secondary effects on O-H (water) and C-H (organic) bonds. This study be considered as a laboratory-scale feasibility study demonstrating the potential of Vis–NIR and SW–NIR spectroscopy combined with chemometric modelling to detect and quantify adulteration in red dragon fruit peel powder, as a highly effective, rapid, and reliable method. These findings lay a solid foundation for the future development of portable and real-time authentication systems for natural food colorants.

ACKNOWLEDGMENTS

The authors gratefully acknowledge the financial support for this Master's Thesis research (2025) from the Ministry of Higher Education, Science, and Technology of the Republic of Indonesia. We also extend our sincere gratitude to the Laboratory of Biophysics Engineering, Department of Agricultural and Biosystems Engineering, Faculty of Agricultural Technology, Universitas Gadjah Mada, for providing laboratory facilities, technical assistance, and the Vis–NIR and SW-NIR spectroscopy instruments used for data collection.

AUTHOR CONTRIBUTION STATEMENT

Author	C	M	So	Va	Fo	I	R	D	O	E	Vi	Su	P	Fu
NHN	✓	✓	✓	✓	✓	✓	✓	✓	✓		✓		✓	
REM	✓	✓		✓	✓		✓			✓		✓	✓	✓
MFRP	✓	✓	✓	✓	✓		✓			✓	✓	✓		
HZA	✓	✓		✓						✓		✓		
RAPH		✓	✓	✓	✓									

C: Conceptualization	Fo: Formal Analysis	O: Writing - Original Draft	Fu: Funding Acquisition
M: Methodology	I: Investigation	E: Writing - Review & Editing	P: Project Administration
So: Software	D: Data Curation	Vi: Visualization	
Va: Validation	R: Resources	Su: Supervision	

REFERENCES

Abadi, F.R., Masithoh, R.E., Sutiarso, L., & Rahayoe, S. (2024). Evaluation of Indonesian local soybean based on chemical characteristics and visible - near infrared spectra with chemometrics. *Biotropia*, ***31***(1), 63–75. https://doi.org/10.11598/BTB.2024.31.1.2054

Amanah, H.Z., Joshi, R., Masithoh, R.E., Choung, M.-G., Kim, K.-H., Kim, G., & Cho, B.-K. (2020). Nondestructive measurement of anthocyanin in intact soybean seed using Fourier Transform Near-Infrared (FT-NIR) and Fourier Transform Infrared (FT-IR) spectroscopy. *Infrared Physics & Technology*, ***111***, 103477. https://doi.org/10.1016/j.infrared.2020.103477

Ambrose, A., & Cho, B.-K. (2014). A review of technologies for detection and measurement of adulterants in cereals and cereal products. *Journal of Biosystems Engineering*, ***39***(4), 357-365. https://doi.org/10.5307/JBE.2014.39.4.357

Batistela, V.R., Pellosi, D.S., de Souza, F.D., da Costa, W.F., Santin, S.M.O., de Souza, V.R., Caetano, W., de Oliveira, H.P.M., Scarminio, I.S., & Hioka, N. (2011). pKa determinations of xanthene derivates in aqueous solutions by multivariate analysis applied to UV–Vis spectrophotometric data. *Spectrochimica Acta Part A: Molecular and Biomolecular Spectroscopy*, ***79***(5), 889–897. https://doi.org/10.1016/J.SAA.2011.03.027

Beć, K.B., Grabska, J., & Czarnecki, M.A. (2018). Spectra-structure correlations in NIR region: Spectroscopic and anharmonic DFT study of n-hexanol, cyclohexanol and phenol. *Spectrochimica Acta - Part A: Molecular and Biomolecular Spectroscopy*, ***197***, 176–184. https://doi.org/10.1016/j.saa.2018.01.041

Chen, R., Li, S., Cao, H., Xu, T., Bai, Y., Li, Z., Leng, X., & Huang, Y. (2024). Rapid quality evaluation and geographical origin recognition of ginger powder by portable NIRS in tandem with chemometrics. *Food Chemistry*, ***438***, 137931. https://doi.org/10.1016/J.FOODCHEM.2023.137931

Dharmawan, A., & Masithoh, R.E. (2025). Authentication of robusta coffee origins by shortwave NIR spectroscopy coupled with dimensionality reduction and neural networks. *International Journal of Agriculture and Biosciences*, ***14***(6), 1291–1301. https://doi.org/10.47278/journal.ijab/2025.110

ElMasry, G., Sun, D.W., & Allen, P. (2011). Non-destructive determination of water-holding capacity in fresh beef by using NIR hyperspectral imaging. *Food Research International*, ***44***(9), 2624-2633. https://doi.org/10.1016/j.foodres.2011.05.001

Eveline, & Audina, M. (2019). Utilization of super red dragon fruit peel (*Hylocereus Costaricensis* (F.A.C. Weber) Britton & Rose) in the making of fermented beverage. *IOP Conference Series: Earth and Environmental Science*, ***292***(1), 012037. https://doi.org/10.1088/1755-1315/292/1/012037

Fernández-Novales, J., López, M. I., Sánchez, M. T., Morales, J., & González-Caballero, V. (2009). Shortwave-near infrared spectroscopy for determination of reducing sugar content during grape ripening, winemaking, and aging of white and red wines. *Food Research International*, ***42***(2), 285-291. https://doi.org/10.1016/j.foodres.2008.11.008

Guo, Z., Huang, W., Peng, Y., Chen, Q., Ouyang, Q., & Zhao, J. (2016). Color compensation and comparison of shortwave near infrared and long wave near infrared spectroscopy for determination of soluble solids content of "Fuji" apple. *Postharvest Biology and Technology*, ***115***, 81-90. https://doi.org/10.1016/j.postharvbio.2015.12.027

Henn, R., Kirchler, C.G., Grossgut, M.E., & Huck, C.W. (2017). Comparison of sensitivity to artificial spectral errors and multivariate LOD in NIR spectroscopy – Determining the performance of miniaturizations on melamine in milk powder. *Talanta*, ***166***, 109–118. https://doi.org/10.1016/J.TALANTA.2017.01.035

Hernanda, R.A.P., Kim, J., Kim, J., Faqeerzada, M.A., Amanah, H.Z., Cho, B.-K., Kim, M. S., & Lee, H. (2024). Spectral analysis for Protaetia brevitarsis seulensis powder adulterated with chickpea (*Cicer arietinum*) and soybean (*Glycine max*) flour by pointed near-infrared spectroscopy. *Korean Journal of Agricultural Science*, ***51***(4), 451–464. https://doi.org/10.7744/kjoas.510404

Huang, C.J., Han, L.J., Liu, X., & Ma, L.J. (2009). Rapid measurement for moisture and calorific value of straw based on near infrared spectroscopy and local algorithm. Hongwai Yu Haomibo Xuebao/Journal of Infrared and Millimeter Waves, 28(3), 184-187. https://doi.org/10.3724/SP.J.1010.2009.00184

Lanjewar, M.G., Asolkar, S., Parab, J.S., & Morajkar, P.P. (2024). Detecting starch-adulterated turmeric using Vis-NIR spectroscopy and multispectral imaging with machine learning. *Journal of Food Composition and Analysis*, ***136***, 106700. https://doi.org/10.1016/J.JFCA.2024.106700

Lohumi, S., Lee, S., Lee, W.H., Kim, M.S., Mo, C., Bae, H., & Cho, B.K. (2014). Detection of starch adulteration in onion powder by FT-NIR and FT-IR spectroscopy. *Journal of Agricultural and Food Chemistry*, ***62***(38), 9246–9251. https://doi.org/10.1021/jf500574m

Lúcia, M., Simeone, F., Parrella, R.A.C., Schaffert, R.E., Damasceno, C.M.B., Leal, M.C.B., & Pasquini, C. (2017). Near infrared spectroscopy determination of sucrose, glucose and fructose in sweet sorghum juice. *Microchemical Journal*, ***134***, 125–130. https://doi.org/10.1016/j.microc.2017.05.020

Lukacs, M., Bazar, G., Pollner, B., Henn, R., Kirchler, C.G., Huck, C.W., & Kovacs, Z. (2018). Near infrared spectroscopy as an alternative quick method for simultaneous detection of multiple adulterants in whey protein-based sports supplement. *Food Control*, ***94***, 331–340. https://doi.org/10.1016/j.foodcont.2018.07.004

Lukacs, M., Vitalis, F., Bardos, A., Tormási, J., Bec, K.B., Grabska, J., Gillay, Z., Tömösközi-Farkas, R.A., Abrankó, L., Albanese, D., Malvano, F., Huck, C.W., & Kovacs, Z. (2024a). Comparison of multiple NIR instruments for the quantitative evaluation of grape seed and other polyphenolic extracts with high chemical similarities. *Foods*, ***13***(24), 4164. https://doi.org/10.3390/FOODS13244164

Lukacs, M., Zaukuu, J.-L.Z., Bazar, G., Pollner, B., Fodor, M., & Kovacs, Z. (2024b). Comparison of multiple NIR spectrometers for detecting low-concentration nitrogen-based adulteration in protein powders. *Molecules*, ***29***(4), 781. https://doi.org/10.3390/molecules29040781

Macavilca, E.A., & Condezo-Hoyos, L. (2020). Assessment of total antioxidant capacity of altiplano colored quinoa (*Chenopodium quinoa* willd) by visible and near-infrared diffuse reflectance spectroscopy and chemometrics. *LWT*, ***134***, 110182. https://doi.org/10.1016/J.LWT.2020.110182

Masithoh, R.E., Hernanda, R.A.P., Amanah, H.Z., Cho, B.K., & Rohman, A. (2025). Nondestructive quantification of betalain secondary metabolites in red beet (*Beta vulgaris*) powder using near- and mid-infrared spectroscopy. *Food Biophysics*, ***20***(1), 26. https://doi.org/10.1007/s11483-024-09915-w

Masithoh, R.E., Pahlawan, M.F.R., Arifani, E.N., Amanah, H.Z., & Cho, B.K. (2024). Determination of the betacyanin and betaxanthin contents of red beet (*Beta Vulgaris*) powder using partial least square regression based on visible-near infrared spectra. *Trends in Sciences*, ***21***(5), 7639. https://doi.org/10.48048/tis.2024.7639

Merzlyak, M.N., Solovchenko, A.E., & Gitelson, A.A. (2003). Reflectance spectral features and non-destructive estimation of chlorophyll, carotenoid and anthocyanin content in apple fruit. *Postharvest Biology and Technology*, ***27***(2), 197–211. https://doi.org/10.1016/S0925-5214(02)00066-2

Monago-Maraña, O., Eskildsen, C.E., Galeano-Díaz, T., Muñoz de la Peña, A., & Wold, J.P. (2021). Untargeted classification for paprika powder authentication using visible – Near infrared spectroscopy (VIS-NIRS). *Food Control*, ***121***, 107564. https://doi.org/10.1016/j.foodcont.2020.107564

Nisa, N.H., Masithoh, R.E., Pahlawan, M.F.R., & Wati, A.T. (2025). Application of machine learning and deep learning to detect adulteration in food flour based on spectroscopy data: A systematic review. *BIO Web of Conferences*, ***192***, 01005. https://doi.org/10.1051/bioconf/202519201005

Pellosi, D.S., Estevão, B.M., Freitas, C.F., Tsubone, T.M., Caetano, W., & Hioka, N. (2013). Photophysical properties of erythrosin ester derivatives in ionic and non-ionic micelles. *Dyes and Pigments*, ***99***(3), 705–712. https://doi.org/10.1016/J.DYEPIG.2013.06.026

Rinnan, Å., van den Berg, F., & Engelsen, S.B. (2009). Review of the most common pre-processing techniques for near-infrared spectra. *TrAC Trends in Analytical Chemistry*, ***28***(10), 1201–1222. https://doi.org/10.1016/J.TRAC.2009.07.007

Rismiwandira, K., Roosmayanti, F., Pahlawan, M.F.R., & Masithoh, R.E. (2021). Application of fourier transform near-infrared (FT-NIR) spectroscopy for detection of adulteration in palm sugar. *IOP Conference Series: Earth and Environmental Science*, ***653***(1), 012122. https://doi.org/10.1088/1755-1315/653/1/012122

Roosmayanti, F., Rismiwindira, K., & Masithoh, R.E. (2021). Detection of coconut (*Cocos nucifera*) sugar adulteration in palm (*Arenga pinnata* Merrill) sugar by Fourier Transform Infrared (FT-IR) spectroscopy. *Food Research*, ***5***(Suppl. 2), 31–36. https://doi.org/10.26656/fr.2017.5(S2).013

Saenjum, C., Pattananandecha, T., & Nakagawa, K. (2021). Antioxidative and anti-inflammatory phytochemicals and related stable paramagnetic species in different parts of dragon fruit. *Molecules*, ***26***(12), 3565. https://doi.org/10.3390/molecules26123565

Sans, S., Ferré, J., Boqué, R., Sabaté, J., Casals, J., & Simó, J. (2018). Determination of chemical properties in 'calçot' (*Allium cepa* L.) by near infrared spectroscopy and multivariate calibration. *Food Chemistry*, ***262***, 178-183. https://doi.org/10.1016/j.foodchem.2018.04.102

Saputri, D.A.S., Pahlawan, M.F.R., Murti, B.M.A., & Masithoh, R.E. (2022). Vis/NIR spectroscopy for non-destructive method in detecting soybean seeds viability. *IOP Conference Series: Earth and Environmental Science*, ***1038***(1), 012043. https://doi.org/10.1088/1755-1315/1038/1/012043

Singh, S., Szostak, R., & Czarnecki, M.A. (2021). Vibrational intensities and anharmonicity in MIR, NIR and Raman spectra of liquid CHCl3, CDCl3, CHBr3 and CDBr3: Spectroscopic and theoretical study. *Journal of Molecular Liquids*, ***336***, 116277. https://doi.org/10.1016/j.molliq.2021.116277

Thalhamer, B., & Buchberger, W. (2019). Adulteration of beetroot red and paprika extract based food colorant with Monascus red pigments and their detection by HPLC-QTof MS analyses. *Food Control*, ***105***, 58–63. https://doi.org/10.1016/j.foodcont.2019.05.020

Vera, W., Salvador-Reyes, R., Quispe-Santivañez, G., & Kemper, G. (2025). Detection of adulterants in powdered foods using near-infrared spectroscopy and chemometrics: Recent advances, challenges, and future perspectives. *Foods*, ***14***(18), 3195. https://doi.org/10.3390/foods14183195

Wang, X., Esquerre, C., Downey, G., Henihan, L., O'Callaghan, D., & O'Donnell, C. (2018). Assessment of infant formula quality and composition using Vis-NIR, MIR and Raman process analytical technologies. *Talanta*, ***183***, 320–328. https://doi.org/10.1016/J.TALANTA.2018.02.080

Xiaowei, H., Liuzi, D., Zhihua, L., Jin, X., Jiyong, S., Xiaodong, Z., Junjun, Z., Ning, Z., Holmes, M., & Xiaobo, Z. (2023). Fabrication and characterization of colorimetric indicator for Salmon freshness monitoring using agar/polyvinyl alcohol gel and anthocyanin from different plant sources. *International Journal of Biological Macromolecules*, ***239***, 124198. https://doi.org/10.1016/j.ijbiomac.2023.124198

Zhang, D., Xu, L., Wang, Q., Tian, X., & Li, J. (2019). The Optimal Local Model Selection for Robust and Fast Evaluation of Soluble Solid Content in Melon with Thick Peel and Large Size by Vis-NIR Spectroscopy. *Food Analytical Methods*, ***12***(1), 136–147. https://doi.org/10.1007/s12161-018-1346-3

Zhang, M., Zhao, C., Shao, Q., Yang, Z., Zhang, X., Xu, X., & Hassan, M. (2019). Determination of water content in corn stover silage using near-infrared spectroscopy. *International Journal of Agricultural and Biological Engineering*, ***12***(6), 143-148. https://doi.org/10.25165/j.ijabe.20191206.4914